[1]Hojjatullah Ghasemi

[2*]Amirpouya Sarraf

[3]Babak Aminnejad

Evaluating Multi-objective Optimization Algorithms to Improve Hydrological Models Using Remote-Sensing Data of Actual Evapotranspiration Values in Karun's Drainage Basin

Abstract: - To enhance basin management and make the most of available water resources, it is essential to determine the real evapotranspiration in drainage basins. The SWAT hydrological model and the SEBAL algorithm for remote sensing are two well-known techniques that deal with this. Initially, the evapotranspiration values of the Karun drainage basin were obtained in three different years—2015, 2019 and 2022—during normal, wet, and dry conditions using the calibrated SWAT model and multi-objective optimization algorithms of BOA and HBA based on the SEBAL algorithm and run-off. Six hydrometric stations were used to calibrate and verify the SWAT model, respectively, for the years 2006–2016 and 2017–2020. The goals of this study included the analysis of applying the multi-objective method to calibrate the SWAT model instead of the traditional method and the assessment of identifying model parameters.

Keywords: Actual Evapotranspiration; SWAT Hydrological Model; Multi-Objective Optimization Model of BOA and HBA; Crop Yield; LandSat; MODIS

INTRODUCTION

One of the main topics in national water resource management is assessing real evapotranspiration in drainage basins to use water resources as efficiently as possible. Because there is less precipitation than what plants require in dry and semi-arid areas, surface waters and groundwater levels must be used for irrigation. Therefore, it is especially important to accurately estimate evapotranspiration in water resources in the agricultural sector. Some research projects such as river basin management and water supply systems have shown that using evapotranspiration point data (using a lysimeter and an eddy correlation device) has not met requirements, and the need for the spatial distribution of actual evapotranspiration is urgent. One of the barriers to managing nationwide water resources has been a shortage of adequate measurement equipment and stations within appropriate statistical periods. To tackle this, computerized simulation has been used to manage drainage basins.

On the other hand, at the drainage basin level, there is a need for a model that would apply a large volume of data, including temperature, precipitation, topographic conditions, soil properties, land use, cultivation models, etc., in addition to using remote-sensing methods. For this, it is critical to use comprehensive methods and models in this connection. Prior research has elaborated on some methods of evapotranspiration estimation across drainage basins using satellite imagery, with the main problems of existing algorithms as well as guidelines for dealing and reducing them have been discussed. In most of this body of research, actual evapotranspiration has been estimated by using MODIS (Ruhoff *et al.* 2012) or LandSat (Wei *et al.* 2012) imagery using the SEBAL algorithm (Bastiaanssen *et al.* 1998, Walters *et al.* 2002), and the results were compared by the standard FAO method with lysimeter values, eddy correlation device, Penman-Monteith and Hargreaves Samani models, agricultural water consumption modeling, pan evaporation values, etc. (Allen *et al.* 1998, Trezza and Allen 2003, Mir Yaeghub Zadeh 2014).

As shown by the research, the MODIS sensing images were found to be appropriate to estimate evapotranspiration at regional and farmland scales, due to desirable daily repetition; meanwhile, LandSat images, with a 16-day temporal resolution ability, would serve well at 30-m spatial resolution on spectral bands and at 60-m spatial resolution on thermal bands, as they can better reveal and separate farmlands (Tasumi *et al.* 2008, Hong *et al.*

[1] PhD Candidate in Water Resources Management and Engineering, Department of Civil Engineering, Roudehen Branch, Islamic Azad University, Roudehen, Iran

[2]Assistant Professor, Department of Civil Engineering, Roudehen Branch, Islamic Azad University, Roudehen, Iran

[3]Assistant Professor, Department of Civil Engineering, Roudehen Branch, Islamic Azad University, Roudehen, Iran

* Corresponding author: Amirpouya Sarraf (Sarraf@riau.ac.ir)

2009). On the other hand, the most conventional direct method is to determine evapotranspiration using the principle of mass balance in a controlled volume of soil (lysimeter). Since it is too costly to install a lysimeter, it is not popular and for this, indirect (computing) methods can be used to estimate evapotranspiration. The FAO Penman Monteith approach is the most reliable indirect method among these. Global research has demonstrated that the evapotranspiration numbers computed using the FAO Penman Monteith technique have higher accuracy than those recorded using lysimeters and other relations. When lysimeter data are lacking, the above method is suggested to be a standard relation. Hydrological models used in simulating drainage basins are also divided into two integrative and distributive groups, with the latter models mainly taking into consideration spatial changes in simulation due to connection to the GIS; however, it is time-consuming to implement them in wider basins (Sarraf and Ghasemi 2022). The first hydrological model is the Stanford model developed by Singh (Singh *et al.* 2009). In recent years, some models of semi-distributive nature have been applied and have worked successfully in simulating wider basins (Sarraf and Ghasemi 2022). One such model, which is applied across the world, is the SWAT (Soil and Water Assessment Tool) hydrological model. The SWAT model was first developed in 1990 by Jeff Arnold et al. at the American Agricultural Research Institute (Arnold *et al.* 1990). Numerous researchers have used and investigated the efficiency of the SWAT model and its capabilities in simulating run-offs, water quality, sediments and evapotranspiration under different climatic and hydrological conditions (Abbaspour 2001). In Iran, the wheat crop yield and agricultural water exploitation were investigated by the SWAT model. According to prior research, the components of the water balance equation were found by comparing the evapotranspiration parameter estimated by the SWAT model with the Energy Balance Algorithm (Immerzeel and Droogers 2008, Mir Yaeghub Zadeh 2014) or by calibrating the results using tools like the PEST non-linear optimization software package. It is noteworthy that most of the research has emphasized the efficiency of the SEBAL algorithm and the SWAT model in evapotranspiration estimation. However, few studies have investigated the simultaneous performance of these two methods in estimating evapotranspiration. The present study aimed to calibrate the SWAT model based on run-off and crop yield, which is directly related to evapotranspiration. The study also developed the SEBAL algorithm using the images of two different sensors, and finally compared their results, which is a strong point of this study.

The Area under Study

The drainage basin of the Karun River is located between longitudes 51°45'E and 48°W and latitudes 29°45' to 32°37'N. The geographical location of this basin lies in southwestern Iran and spans large swathes of the country, including the provinces of Chahar Mahal Va Bakhtiari, Khuzestan, Yasuj, Kohgiluyeh Va Boyer Ahmad, Isfahan, Lorestan and Hamedan (Khodabakhsh *et al.* 2016). The big Karun is a permanent river measuring 890 km long with an area of 67255 km2, accounting for around 5% of the total Iran's area. In addition, it has an average dip of 0.3%, an average annual discharge of 575 m3/s and an average annual rainfall of 600 mm. The big Karun River, which carries the largest volume of water and is the highest river in Iran, originates from the foothills of Mt. Vang and Zard Kuh, located in Shurab Village, some 92 km northwest of Shahre Kord. After passing through the villages of the city of Shahre Kord, the river enters the villages of Boroujen, Lordegan, Izeh and Masjed Soleiman before entering the Persian Gulf after passing through the cities of Shushtar, Ahvaz and Khorramshahr. Figure 1 shows the location of the drainage basin branch of Karun in the province of Khuzestan.

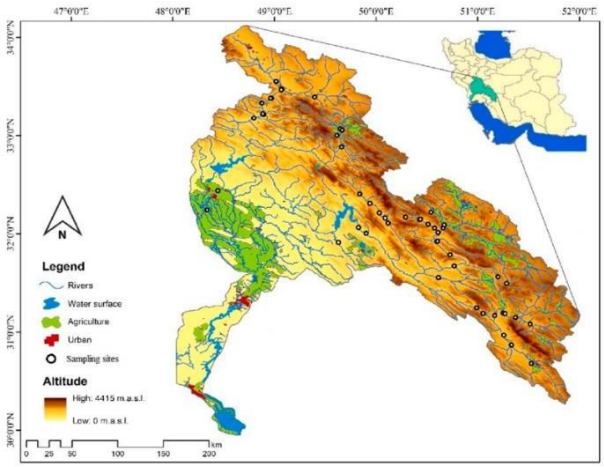

Figure 1. Area under study.

Materials and Procedure

In this study, in order to produce a network of waterways and sub-basins, a DEM (Digital Elevation Model) map by the Aster Satellite of Khuzestan with an accuracy of 5 meters was used. In addition, a land use classification map of global land vegetation with an accuracy of 1 km and a classification map of soil with an accuracy of 5 km were used. Meteorological data to be used in the SWAT model were taken from the National Meteorological Organization and the NASA meteorological database, as well as synoptic stations from 1979 to 2022. The data included precipitation, temperature, the angle and direction of radiation, the speed and direction of wind, soil moisture and monthly run-off data, taken from hydrometric stations. Meanwhile, due to the vastness of the drainage basin and the lack of stations around it, the data of the neighboring stations that provided information on the main branches (main tributaries) were used. The location of these station is shown by Figure 2.

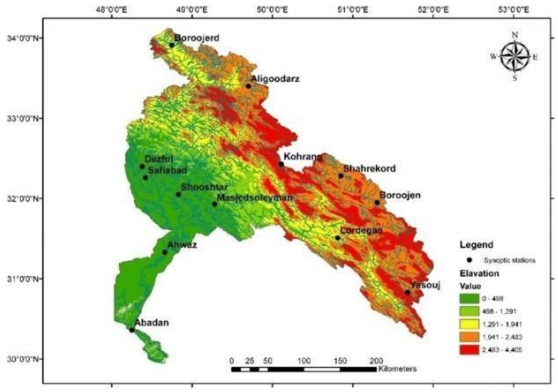

Figure 2. Location of meteorological and hydrometric stations.

To implement the SEBAL algorithm in this study, it was required to have a set of satellite imagery data, regional DEM and meteorological data. In the first stage, MODIS sensing data, taken from the Terra satellite, were used to extract satellite data. MODIS sensing images are accessible as MODIS crops at two different levels. First-level data are raw satellite data, while second-level data are data extracted from such LST, NDVI, etc. satellites. As well, to produce the required DEM in the SEBAL algorithm Aster GDEM data were used. Table 1 gives the crops required by the MODIS sensor and the relevant indices that can be extracted to run the SEBAL model.

Table 1. Satellite imagery and crops for the SEBAL model.

Indirect extractable index	Extractable index	Title
Land Surface Temperature Leaf Area Index (LAI) Albedo	Surface Reflectance Emissivity	MOD09A1 500m
Vegetation Indices	Sun Elevation Sun Zenith Angle	MCD64A1
-	DEM	Aster – Dem
NDVI – LST – Albedo	Reflectance – Radiance	Landsat 8

MODIS sensing data of the entire Karun basin are extracted by selecting the type of the crops, time periods, and the location, as Aster GDEM satellite data, with a 5-m spatial resolution power, would be accessible after selecting the areas under study and setting relevant adjustments. The produced satellite data will be used after being extracted and decided upon. At this stage, for every twelve months of each of the three years (stated above), images of the day when evaporation, as recorded by meteorological station data, was the highest (a total of 36) were downloaded, and the SEBAL algorithm. was run to calculate the evapotranspiration values. It should be stated that the required meteorological data were obtained from 46 stations and pertained to three normal, dry and wet years. At the second stage, OLI sensing images by the LandSat 8 Satellite of the Al-Baji plain (2020/11/07) and MODIS sensing images by the Terra plain of the Molla Sani plain (2017/11/15) were used. Ground data required for this stage are as follows (Table 2).

Table 2. Ground data used in the second stage.

Type of images	Dates	Temperature (°C)	Wind speed	Average elevation (m)
Landsat 8	2020/11/07	30	5	1700
MADIS	2017/11/15	34	3	850

A hypothetical plant with a height of 0.12 m, a surface resistance of 70 s/m, and an albedo (reflection coefficient) of 0.23 was used to define the reference plant for the FAO Penman Monteith method. Its evaporation is very similar to that of the vast surface of green grass with uniform height, active growth, and accessibility to enough water. Using this strategy, the prior shortcomings are eliminated and the amount of water utilized by plants is brought closer to the global data measured. Equation 1 provides an estimate of the reference evapotranspiration using the FAO Penman Monteith:

$$ET0 = \frac{408\Delta(Rn-G)+\gamma\frac{900}{T+}u_2(e_s-e_a)}{\Delta+\gamma(1+0.34u_2)} \quad (1)$$

SWAT Model Structure

The SWAT model is a conceptual and semi-distributive model and one of the most popular hydrological models, widely used in formulating flows at different time series. This model provides basin topography, land use and soil maps to develop hydrological response units (HRUs) and simulates run-offs and crop yields. The SWAT model uses the following hydrological balance equation (Equation 2) to simulate hydrological cycles:

$$\Delta SW = \sum_{i=1}^{t}(R_{day} - Q_{surf} - E_a - W_{seep} - Q_{gw}) \quad (2)$$

The studied drainage basin consists of 37 sub-basins and 285 HRUs. The volume of the surface run-off caused by rainfall has been one of the main variables of river flows, and the SWAT model uses the SCS method based on precipitation, land topography, type of land use, soil and previous soil moisture to simulate that variable. The SWAT model also uses balance equations to determine the groundwater share and empirical relations to estimate snow melting to calculate the total amount of run-off (Hooghoudt 1940). Because the evapotranspiration simulation results were quite concrete and could be applied by authorities across the province (Khuzestan), the 1979-2022 data, which were close to those of the present time, were selected for decision-making approaches, as they were demonstrated to be much more efficient. The potential evapotranspiration simulation in the SWAT model was performed in accordance with the Hargreaves Samani method. Actual evapotranspiration is directly related to crop yield, and the stages of simulating and calculating are performed based on a simplified state of the EPIC plant growth model and after setting the crop calendar and effective parameters, in line with existing documents, where the plant's growth is simulated based on the daily cumulative heat received. In the EPIC, the potential of the substance produced by the Monteith method is calculated and the harvesting index for the crop is also calculated. According to this model, the plant is limited based on the lack of temperature, water and fertilizer. To simulate the crop yield, the SWAT model considers a wide range of factors such as meteorological, vegetable and agricultural variables. To simulate actual evapotranspiration, the stages of crop growth are introduced to the model, and the model, prior to estimating the evaporation of soil and transpiration of the plant, will calculate the level of evaporation of the water stored in vegetation based on the leaf area index (LAI), which is a function of the heat reached to the crop during its growth period.

Optimization Algorithms

An advantage of using several goodness-of-fit functions simultaneously is to use various information sources and deal with various dimensions of the process of producing run-off and simulating the output hydrographs of the basins, which eventually decreases simulation uncertainty. In recent years, multi-objective evolutionary algorithms have been used due to the complexity and large-scale nature of the multi-objective calibration of precipitation-run-off models.

Honey Badger Optimization Algorithms (HBA2)

2 New metaheuristic algorithm for solving optimization problem

The Honey Badger Algorithm (HBA) simulates a honey badger's foraging behavior. The honey badger uses its sense of smell to locate food sources, and it either follows the bird that is searching for honey or digs. The states that follow are referred to as the honey state and the digging state, respectively. In the first condition, the honey badger locates its prey by using its sense of smell. Once it has located the prey, it circles around it to choose a good spot to dig and seize it. In the second condition, the honey badger locates the hive on its own after receiving guidance from the bird that seeks honey (Kashef-Hossein *et al.* 2022). Phases of exploration and exploitation are theoretically available to the HBA. As a result, one may consider it to be an algorithm for global optimization. The following is a mathematical breakdown of the suggested HBA stages: Following is a display of the population of the chosen solutions in the HBA:

$$\text{Population of Selected Solutions} = \begin{matrix} x11 & x12 & x13 & \cdots & x1D \\ [x21 & x22 & x23 & ... & x2D] \\ xn1 & xn2 & xn3 & \cdots & xnD \end{matrix}$$

$xi = [X_{i}^{1}, x_{i}^{2}, \cdots, X_{i}^{D}]$ The ith state of the honey badger

Stage 1: Initializing phase: Determine the number of honey badgers (the size of the N population) and their relative states based on Equation (1):

$$Xi=lbi+r1\times(ubi-lbi) \quad (3)$$

Where r1 is a random number between 0 and 1.

Stage 2: Define intensity (I): How focused the prey is and how far away it is from the honey badger determine how intense the attack will be. One's movement will be faster if they can smell the prey strongly, and vice versa. This is known as Ii. For [intensity], Equation (2) defines it according to the inverse square law (Kashef Hossien *et al.* 2022).

$$Ii=r_2 \times s/4\pi di2 \quad (4)$$

$$S = (x_i - x_{i+1})^2$$

$$d_i = x_{prey} - x_i$$

R_2 is a random number between 0 and 1.

Stage 3: Update the density factor: A seamless transition from the exploration to the exploitation stages is ensured by controlling the time-varying randomization through the density factor (α). As time goes on, iteratively reduce randomization by updating the decreasing factor of α using Equation (5):

$$\alpha= C\times\exp(-t/t_{max}) \quad (5)$$

t_{max} is the maximum number of iterations.

Stage 4: Escape the desirable local limit: This stage and the next two ones can be used to escape the optimal region. This study sees the recommended algorithm using a flag (F), as noted from Figures 3 and 4, which accurately changes the direction of the search to make the above opportunities accessible for the factors in order to scan the search for the place.

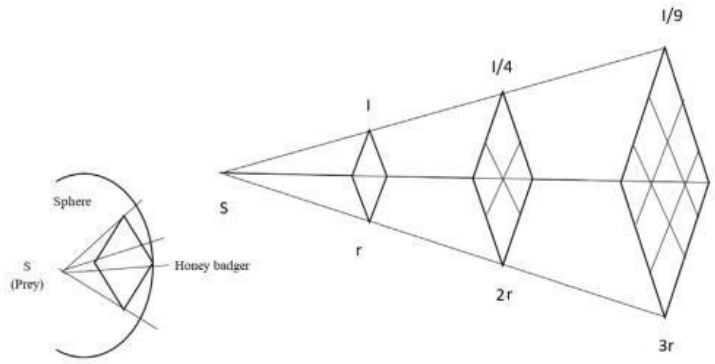

Figure 3. Inverse square law, I is numbness and S is the place of hunting.

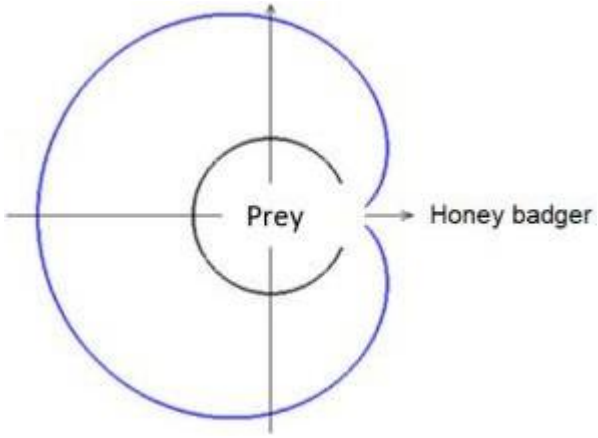

Figure 4. Exploration phase: the outer blue line is the intensity of the smell, and the black one the surrounding place.

Stage 5: Update states of factors: As stated previously, the process of updating the state of HBA (Xnew) is divided into two parts, which include the "exploration" and the honey" phases. Later, a better definition is provided.

Stage 5-1: Exploration stage: The honey badger exhibits behavior resembling a cardioid shape [2] during the exploring period, as seen in Figure 3. Equation (6) can be used to model the cardioid action.

$$x_{new} = x_{prey} + F \times \beta \times I \times x_{prey} + F \times r_3 \times \alpha \times d_i \times |\cos(2\pi r_4) \times [1 - \cos(2\pi r_5)]| \quad (6)$$

Where Xprey is the state of the prey, found in the best global state up to now and F is the flag that changes the direction of the search and is determined by using Equation (7):

$$F = \begin{cases} 1 & \text{if } r_6 \leq 0.5 \\ -1 & \text{else,} \end{cases} \quad (7)$$

R6 is a random number and is between 0 and 1.

Stage 5-2: The honey phase: This condition, which may be replicated using Equation (7), occurs when a honeyseeking bird is followed by a honey badger to reach the hive:

$$x_{new} = x_{prey} + F \times r_7 \times \alpha \times d_i, r_7 \text{ is a random number between 0 and 1}$$

The recommended pseudo-code in the algorithm includes population initialization, population assessment, and parameter updating (Figure 5).

Set parameters t_{max}, N, β, C.
Initialize population with random positions.
Evaluate the fitness of each honey badger position x_i using objective function and assign to f_i, $i \in [1, 2, ..., N]$.
Save best position x_{prey} and assign fitness to f_{prey}.
while $t \leq t_{max}$ **do**
  Update the decreasing factor α using (3).
  for $i = 1$ to N **do**
    Calculate the intensity I_i using Eq. (2).
    if $r < 0.5$ **then** ▷ r is random number between 0 and 1
      Update the position x_{new} using Eq. (4).
    else
      Update the position x_{new} using Eq. (6).
    end if
    Evaluate new position and assign to f_{new}.
    if $f_{new} \leq f_i$ **then**
      Set $x_i = x_{new}$ and $f_i = f_{new}$.
    end if
    if $f_{new} \leq f_{prey}$ **then**
      Set $x_{prey} = x_{new}$ and $f_{prey} = f_{new}$.
    end if
  end for
end while Stop criteria satisfied.
Return x_{prey}

Figure 5. HBA algorithm pre-code.

Billiards-inspired Optimization Algorithm (BOA)

Billiards Algorithm Mechanism

Inspired by the game of pool, the meta-heuristic (BOA) algorithm was created. This method may be thought of as a multi-dimensional game of pool since it solves a problem with several decision-making factors. In reality, these balls represent factors in optimization problems, each of whose diameters presents a variable. In sum, the problem-solution process begins by considering the initial random distribution of the balls. The balls are then separated into two groups: regular and cue balls. A few of the best are then chosen to serve as pockets. Every time a cue ball strikes a target ball, it causes the balls to go toward the pockets. When the cue ball collides with the rest of the balls, the collision and kinematic laws will apply. These rules will dictate how the colliding balls move and end up positioned. In pool, the impact of two balls colliding is nearly elastic. The kinetic energy of the balls is preserved both before and after the contact in a perfect elastic collision, in addition to the momentum. The forces that result from two balls colliding will point in the direction of a virtual line, or line of impact, that joins their centers. In order to clarify, consider that velocity vectors in an impact are separated into two parts: vertical and parallel. The first component is perpendicular to the ball's path of impact, whereas the second is parallel to it. When the balls hit each other, the connection vector $(\overrightarrow{m_1 m_2})$ is drawn from the center of the first ball to the center of the second ball. The connection vector's unit vector can be expressed as the following formulas: The following is how impact velocity's parallel and vertical components are stated (Figure 6):

$$\vec{e}_{\parallel} = \frac{\overrightarrow{m_1 m_2}}{r_1 + r_2}$$

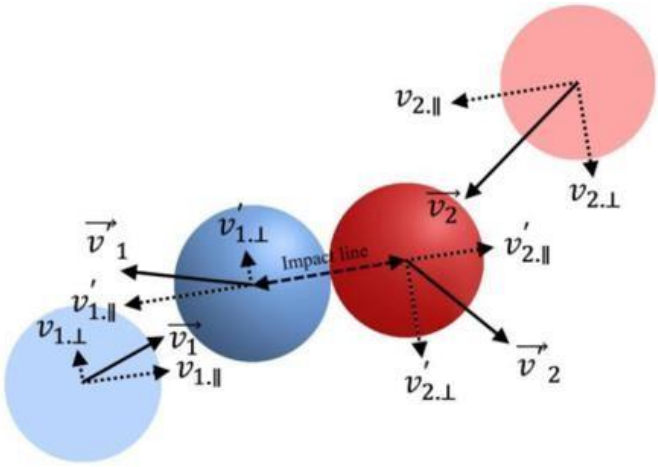

Figure 6. Dividing of velocities into parallel and vertical components.

Where v_1 and v_2 represent the velocities of the first and the second balls prior to the collision and v_1' and v_2' represent the [balls'] velocities before the collision. Also, symbols $||$ and $\perp$ respectively represent parallel and vertical components, while Parameters m_1 and m_2 represent the mass of the balls.

The pseudo-code of the BOA algorithm is shown in Figure 6 and whose steps are as follows (Figure 7).

```
set N=number of balls;
    M=number of variables
    K= number of pockets;
    ET= escaping threshold;
    iter=0;
Initialize 2N balls and K pockets by Eq. (19);
while (iter< iteration limit)
   Evaluate balls and pocket position according to objective
function;
   Update pocket memory and population;
   Create ordinary ball and cue ball groups;
   for each pair ball
      Select a destination pocket by utilizing the roulette-wheel
selection mechanism;
   end
   Update position of current ordinary ball by Eq. (22);
   Calculate velocity of ordinary ball after collision by Eq. (23);
   Calculate velocity of cue ball after collision by Eq. (25);
   Update position of current cue ball by Eq. (26);
   if (rand<ET)
      Regenerate a random dimension of balls by Eq. (27);
   end
      Check the boundary condition limitations and correct the
balls if they are not within the defined range;
   iter=iter+1;
end
Return the best pocket as final solution.
```

Figure 7. Pre-code of the BOA.

Step 1: Initialization

The initial population of the balls is randomly distributed in the search space as follows:

$$B_{n.m}^{0} = var_m^{min} + rand_{[0,1]}(var_m^{max} - var_m^{min}). \quad n = 1.2.\ 3... \quad 2N; \quad m = 1.2.\ 3...M$$

Step 2: Evaluation

The goal function is used in this stage to evaluate the locations of the balls and the pockets.

Step 3: Determine pockets

The pockets in the BOA have two purposes. First, they operate as targets for the balls that are used to extract the algorithm; second, they act as memory, holding the first K numbers of the highest answers that have been identified up to this point. This memory's existence improves the algorithm's efficiency without adding to its computational burden. This memory is refreshed after every iteration, and the balls that are discovered in the best placements are swapped out.

Step 4: Ball grouping

After the pockets were determined, the balls are grouped based on their characteristics and are divided into equal groups of ordinary and cue balls. The first half consists of ordinary balls, i.e., (n=1, …, N) and the second half consists of cue balls, i.e., (n=N+1, … ,2N). Each cue ball belongs to its equivalent in the first half. This method of grouping uses the CBO method.

Step 5: Assign the pockets to the balls

A target pocket is chosen for a regular ball using the roulette wheel selection mechanism. It is more ideally expressed when there are pockets with lower objective function values. The recommended probability function to select a pocket is as follows:

$$P_k = \frac{e^{-\beta f_k}}{\sum_k e^{-\beta f_k}}; \quad k = 1,2,...,K$$

Where the selection pressure is larger than zero and the fk is the value of the objective function for the Pocket k, therefore, increasing the probability of selecting a more effective pocket. Now, the current cue ball hits a target ball and moves t in the direction of the pocket.

Step 6: Update ball positions

The new position of ordinary balls will be around their pockets, after the collision. These positions depend on the accuracy of the impact. Meanwhile, the line in the process of the search decreases in order to improve the ability of the algorithm extraction.

The following equation determines the position of the ordinary balls.

$$B_{n.m}^{new} = rand_{[-ER,ER]}(1 - PR)(B_{n,m}^{old} - P_{k,m}^{n}) + P_{k,m}^{n}, \quad n = 1.2.\ 3...N$$

$$PR = \frac{iter}{iter_{max}}$$

Step 7: Avoid local trap

The BOA mechanism has an inherent exploratory nature. In addition to avoiding falling prey to the local trap (mature convergence), there is an exit threshold like ET in a (0,1) interval, which determines whether or not a dimension (variable) of the updated ball should change. As for any updated ball, ET is compared to rand, which is a random number uniformly distributed in the (0,1) interval. If rand<ET, a random dimension of the updated ball is reconstructed as follows:

$$B_{n.m} = var_m^{min} + rand_{[0,1]}(var_m^{max} - var_m^{min})$$

Step 8: Investigate limitations of boundary conditions

The ultimate location of the balls may be computed outside of the specified range during the process of updating their position. This implies that there's a chance that [the balls] won't fall within the pool table. The ball's dimension crossing the boundary requirements has to be adjusted under this scenario.

Step 9: Investigate the stop criterion

When a predetermined threshold, such as a predetermined number of iterations, is met, the search process comes to an end. The search process ends when the condition is met and the best solution—that is, the best pocket—is found; if not, the search process carries on.

Process of Sentiment Analysis, Calibration and Validation of the SWAT Model

Calibration helps to correct sensitive parameters in a model in a way that the output results get closer to observational data which would be achieved by the iterative changing of the parameters. However, since this is time-consuming, there is a need for an intermediary program. For this, the SWAT-CUP program was developed. This study used the SUFI-2 method from the SWAT-CUP program. This method takes into consideration all uncertainties, including input uncertainty, the conceptual model, parameters and measured data in modeling (Abbaspour 2011). After calibrating the model, it is time to validate it. In validation, simulated data, after being calibrated, will be compared to observational data in a different interval to help determine reliability and validity. To determine the model's accuracy at calibration and validation stages, various statistical indices such as R2, NS and RMSE were used (Equations 8-10; Abbaspour

$$R^2 = \frac{[\sum_{i=1}^{n}(Qm,i - \bar{Q}m)(Qs,i - \bar{Q}s)]^2}{\sum_{i=1}^{N}(Qm,i - Qm)^2 \sum_{i=1}^{N}(Qs,i - Qs)^2} \quad (8)$$

$$NS = 1 - \frac{\sum_{i=1}^{N} (Qs_i - Qo_i)^2}{\sum_{i=1}^{N} (Qo_i - \bar{Qo})^2} \quad (9)$$

$$RMSE = \sqrt{\frac{\sum_{i=1}^{N} (Qs_i - Qo_i)^2}{N}} \quad (10)$$

Where n is the number of observations, Qm and Qs are respectively the measured and estimated run-off values, and $\overline{Qm}$ and $\overline{Qs}$ are respectively the average measured and estimated run-off values.

SEBAL Algorithm

SEBAL is an image processing model that uses digital image data from remote-sensing satellites that monitor visible, near-infrared, and thermal infrared radiation to compute evapotranspiration and other energy transformations on Earth's surface. Utilizing the instantaneous energy balance on the surface of each pixel in a satellite picture, this model calculates the plant's evapotranspiration and is a dependable technique for estimating evapotranspiration at the rural and regional levels. Based on the energy balance is the SEBAL model. In order to estimate evapotranspiration (ET), or the remaining Earth's surface energy balance, 25 models make up the image processing model SEBAL. This model was developed by Bastiaanssen in the Netherlands and used for the mountainous regions of Idaho by considering evapotranspiration values measured on Earth's surface. The SEBAL model uses digital image information obtained by the LandSat satellite or other remote-sensing images, which are capable of recording thermal infrared and also visible and near infrared radiation. The ET value in each pixel (e.g., 30*30 m2 TM and ETM images of LandSat images) is calculated for a special moment, when the same image is obtained. The process of calculation is based on the complete energy balance where the ET value is calculated from deducting the residual energy value of the classic energy balance equation. More details of this model were presented by Bastiaanssen et al. However, the general equation used by SEBAL is as follows.

$$\lambda ET = R_n - H - G \quad (11)$$

Where G is the heat flux of soil or ground (w/m2), H is the sensible heat flux (w/m2), Rn is the net solar reflection (w/m2), and ET is the latent heat flux (w/m2). The implication of this formula is that the radiation from the atmosphere that reaches the Earth's surface is split into three distinct components: the first component heats the ground or soil, the second component heats the air near the surface, and the remaining portion converts to evapotranspiration. In fact, the goal of SEBAL is to calculate the latent heat flux (ET), which is the actual ETY. It should be reminded that the actual accuracy of the results obtained pertain to LE and ET. In the following equation, the net radiation is calculated from Earth's surface energy balance:

$$R_n = (1-\alpha)\, R_s + (L_{in} - L_{out}) \quad (12)$$

The soil heat flux or G can be empirically estimated and by using the Bastiaanssen et al., equation. Details of how the parameters are calculated can be found in the SEBAL manual. In addition, after the data required by the SEBAL algorithm were presented and the equations available in the manual were used, the level of evapotranspiration in the Erdas and Envi software were calculated.

Results and Discussion

Evaluating the SWAT model

The data used by the SWAT model were collected from 1979 to 2022 and included values of temperature, precipitation, the angle and direction of radiation, the speed and direction of wind, and soil moisture. The period of time (1979 to 2022) was considered as the warm-up period for the model. The model, having been implemented, had its output model stored for the studied year to be transferred to the SWAT-CUP software for calibration and validation, as parameter values were obtained using the SUFI_2 algorithm. As stated, calibration corrects the sensitive parameters in the model in a way that the model results become closer to observational and initial data. The SWAT-CUP program was used to avoid the non-uniformity of the parameters. The SWAT-CUP program can be used to calculate the conceptual model of the data, the measurement data, the weighted averaging, as well as the validation and calibration of the parameters. Firstly, the observed and simulated discharge values for the years 1979 to 2017 as well as the parameters affecting the discharge were introduced to the software and a range of standard changes were determined for each of those parameters. In the validation stage, observational and simulated discharge values for the years 2018 to 2022 were used to determine the validity of the model's efficiency. In this stage, initial data were compared to the simulated data to determine the model's validation. In the next stage, all the effective parameters were introduced to the validation and the output results were stored.

One of these calibrated variables is run-off in which effective values are identified and validated and are classified based on the level of weight and validation. After calibrating the run-off, observational and simulated values of the crop (wheat) yield and the actual evapotranspiration were evaluated, eventually leading to the determination and scoring of the effects of major parameters in simulation, along with p-value and t-stat values. Any parameter with a higher or lower absolute value will be considered the most effective ones. Tables 3, 4 lists the parameters affecting the run-off at the order of sensitivity.

Table 3. Parameters affecting the run-off.

Parameter name	Parameter concept	P-Value	t-Stat	Final range and calibrated value
OV_N. hru	Manning's coefficient value of surface flow (dimensionless)	1.30	0.35	25-4
RCHRG_ DP.gw	Deep aquifer infiltration fraction	0.25	0.76	0.0-10.49
ALPHA_BF. gw	Baseflow response coefficient for groundwater (per day)	0.74	0.50	0.0-25.82
LAT_TTIMF .hru	Time efficiency of lateral flow (day)	0.93	0.39	-2.105-59.65
GWQMN.gw	Minimum elevation of the waters stage required for water exit (mm)	0.59	0.58	2038.1804
SOL_K (1) sol	Hydraulic conductivity of soil saturation on the surface layer (mm/hour)	0.45	0.75	-1.0-15.29
SOL_AWC (1).sol	Accessible water coefficient of the soil on the surface layer (mm/m)	2.11	0.19	-0.0-60.60
PLAPS.sub	Precipitation rate (mm/km)	1	0.4	-65.227
ESCO.hru	Soil evaporation compensation factor (dimensionless)	0.29	0.75	-0.1-43.2
SLSUBBSN. hru	Average dip length (m)	1.45	0.22	49-11
HRU_SLP.hr u	Average dip (m/m)	0.83	0.41	0.0-26.75
GW_DELAY .gw	Delay time of water infiltration to the water stage (days)	0.03	0.93	0.0-26.75
CH_N2.rte	Manning's coefficient of the main river (dimensionless)	0.35	0.84	0.0-04.13
CH_K2.rte	Effective hydraulic conductivity of the main river (mm/hour)	0.69	0.49	1.7-52.23
REVAPMN. gw	Water threshold depth in the shallow aquifer to cover or infiltrate to the deep aquifer (mm)	0.6	0.54	135.52
SOL_BD (1).sol	Apparent soil density on the surface layer (g/cm3)	0.39	0.54	0.24
CN2.mgt	Infiltration curve number under average humidity conditions (dimensionless)	0.53	0.69	72.33

Table 4. Values of model evaluation indices at the stages of calibration and validation.

Stages	Index title	Values obtained from each station					
		Ab Ganji	Ahvaz	Hamid	Khosrawi	Ahvaz Shahid Chamran University	Umrah
Pre-calibration	R2	-0.06	-0.07	-0.05	-0.08	-0.12	-0.06
	NS	0.52	0.55	0.48	0.49	0.60	0.54
	RMSE(m3/s)	22.26	19.50	20.07	41	35.03	45
Calibration	R2	0.64	0.67	0.54	0.60	0.71	0.55
	NS	0.62	0.63	0.54	0.57	0.68	0.52
	RMSE(m3/s)	17.26	12.50	12.50	32	16.08	24.96
	R2	0.60	0.63	0.53	0.57	0.65	0.51

Validation	NS	0.58	0.61	0.52	0.54	0.65	0.50
	RMSE(m3/s)	12.63	12.63	12.03	13.11	16.03	23.23

Zoning and Modeling of Evapotranspiration Using IDW

After calculating evapotranspiration by the SWAT model, its average values were calculated, and the IDW method and the GIS software were used to prepare the map of the evapotranspiration zoning in the months and years under study. In the IDW zoning method, weights are assigned to the neighboring z points relative to their distance from the unknown point and are inserted into the equation. In fact, there will be a kind of weighted averaging, i.e.,

$$w\alpha\frac{1}{d_i^p}$$

The following figures exhibit the maps of the evapotranspiration zoning of Karun's drainage basin using the IDW method and the output results of the SWAT model in spring (from left to right respectively) in three rows pertaining to 2019 (dry), 2020 (normal) and 2021 (wet), as given from top to bottom, respectively. In addition, maps of other seasons, including summer, autumn and winter are shown (Figures 8-11).

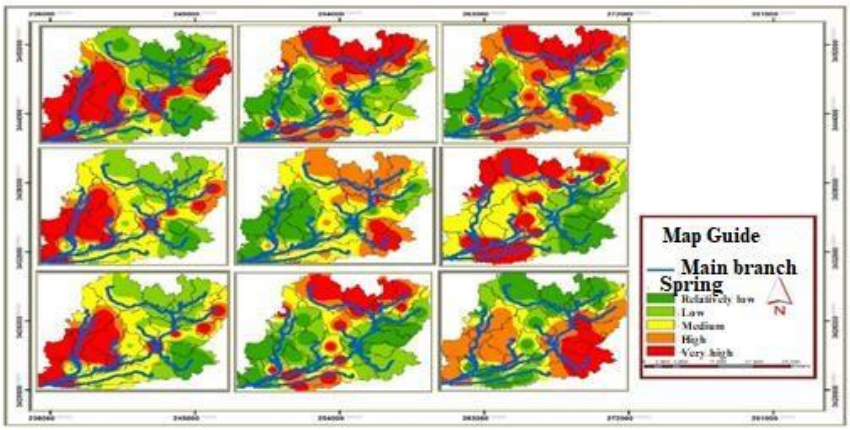

Figure 8. Map of actual evapotranspiration taken from the SWAT model pertaining to the months of spring (respectively from left to right) in three rows pertaining to 2019 (dry), 2020 (normal) and 2021 (wet) (respectively from top to bottom).

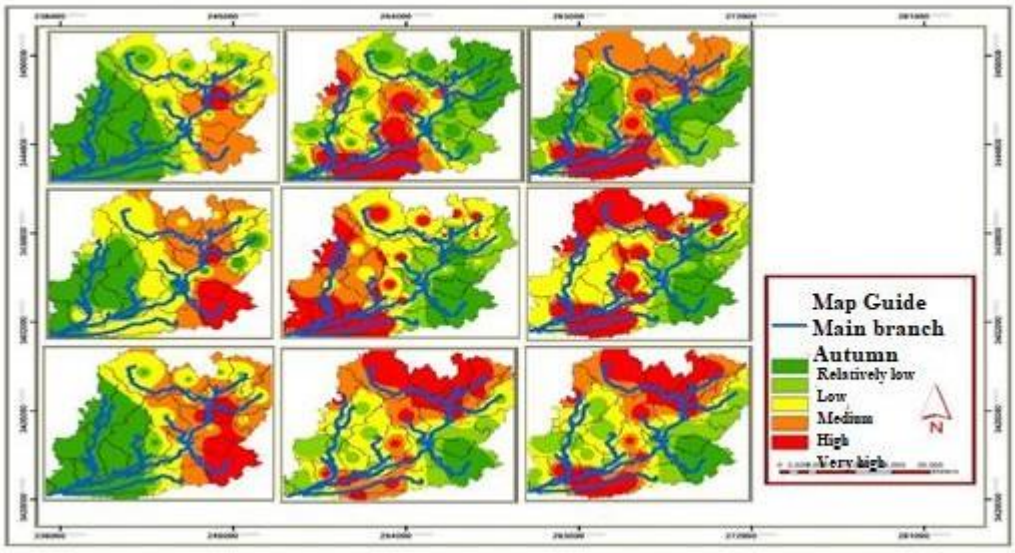

Figure 9. Map of actual evapotranspiration taken from the SWAT model pertaining to the months of autumn (respectively from left to right) in three rows pertaining to 2019 (dry), 2020 (normal) and 2021 (wet) (respectively from top to bottom).

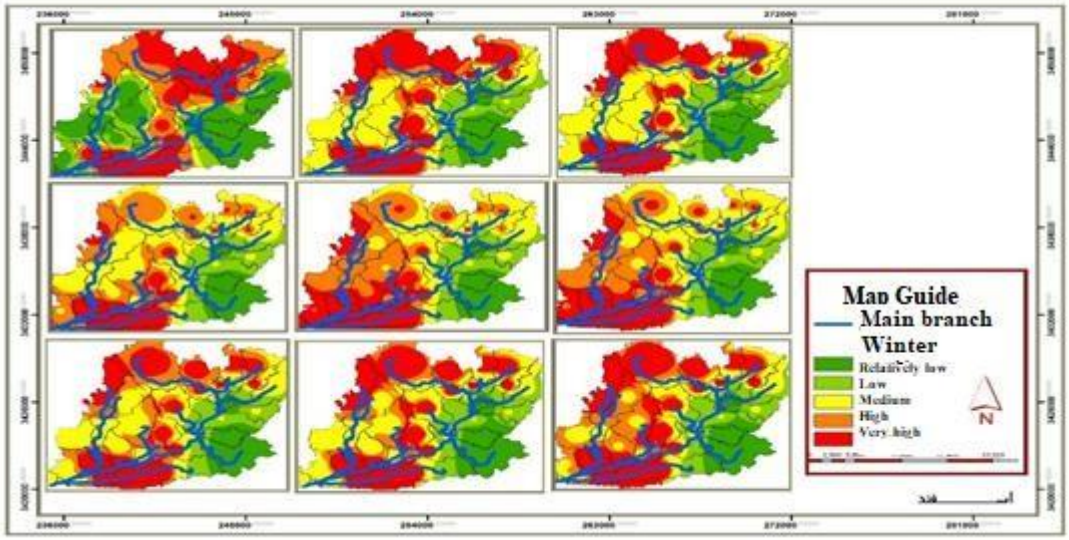

Figure 10. Map of actual evapotranspiration taken from the SWAT model pertaining to the months of winter (respectively from left to right) in three rows pertaining to 2019 (dry), 2020 (normal) and 2021 (wet) (respectively from top to bottom).

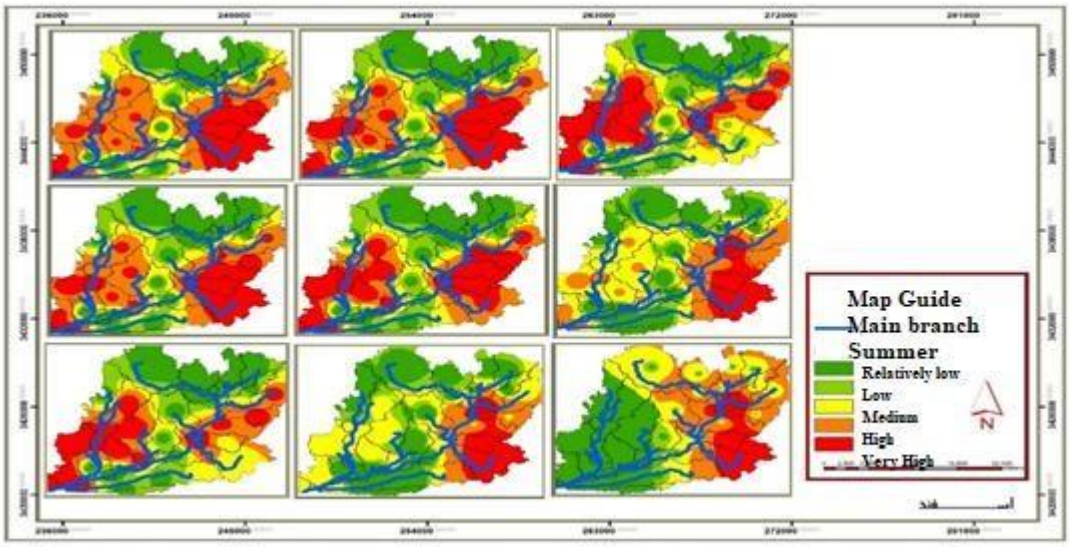

Figure 11. Map of actual evapotranspiration taken from the SWAT model pertaining to the months of summer (respectively from left to right) in three rows pertaining to 2019 (dry), 2020 (normal) and 2021 (wet) (respectively from top to bottom).

By looking at the zoning map of Karun's drainage basin's evapotranspiration, it was revealed that the eastern zones of the basin, as compared to the western zones, saw greater levels of area and evapotranspiration; also, the evapotranspiration values of the studied years in the four seasons were calculated and stored, and the IDW method was used to obtain the zoning maps.

SEBAL Algorithm Results

The following figures exhibit the zoning maps of Karun's drainage basin's evapotranspiration using the IDW method and the output results of the SEBAL model in spring (respectively from left to right) in three rows pertaining to 2019 (dry), 2020 (normal) and 2021 (wet), as given from top to bottom, respectively. As well, the maps of other seasons such as summer, autumn and winter are given, which are listed below (Figures 12-15).

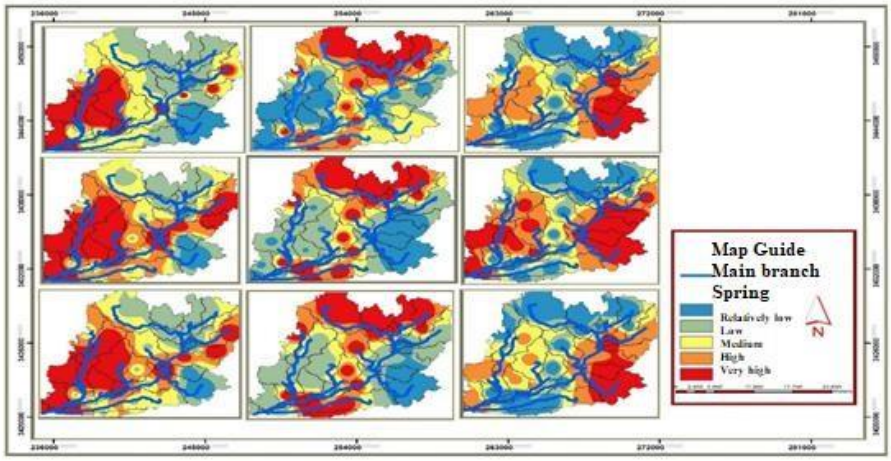

Figure 12. Map of actual evapotranspiration taken from the SEBAL model pertaining to the months of spring (respectively from left to right) in three rows pertaining to 2019 (dry), 2020 (normal) and 2021 (wet) (respectively from top to bottom).

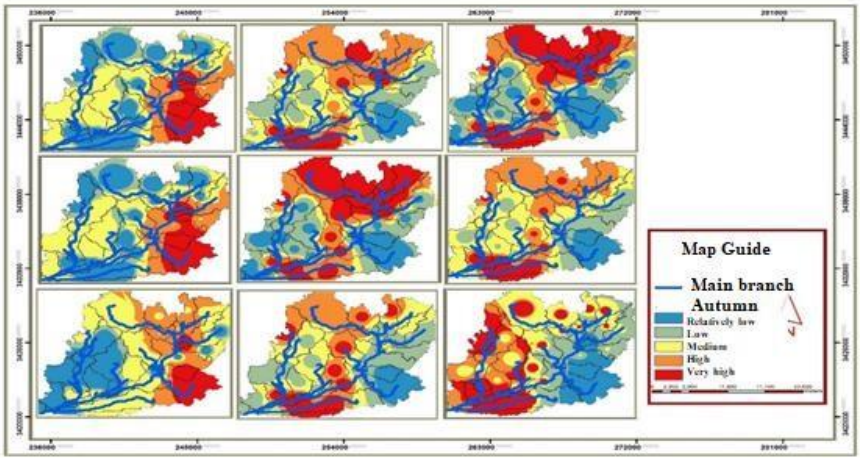

Figure 13. Map of actual evapotranspiration taken from the SEBAL model pertaining to the months of autumn (respectively from left to right) in three rows pertaining to 2019 (dry), 2020 (normal) and 2021 (wet) (respectively from top to bottom).

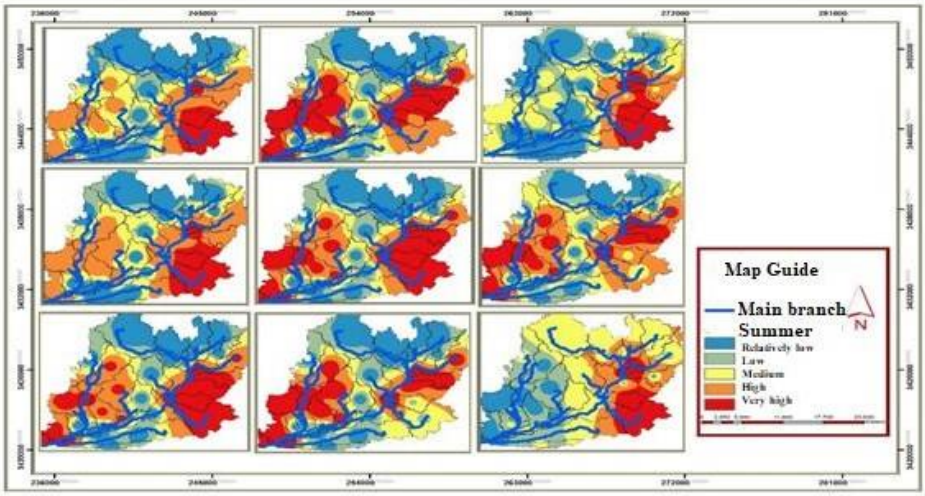

Figure 14. Map of actual evapotranspiration taken from the SEBAL model pertaining to the months of summer (respectively from left to right) in three rows pertaining to 2019 (dry), 2020 (normal) and 2021 (wet) (respectively from top to bottom).

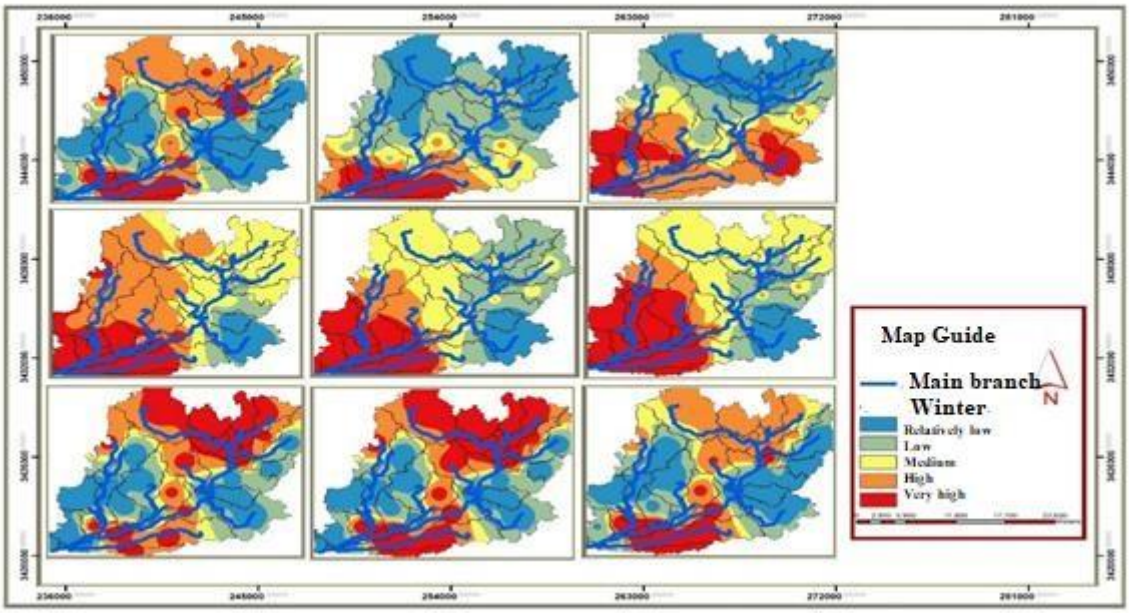

Figure 15. Map of actual evapotranspiration taken from the SEBAL model pertaining to the months of winter (respectively from left to right) in three rows pertaining to 2019 (dry), 2020 (normal) and 2021 (wet) (respectively from top to bottom).

To compare the results of actual evapotranspiration estimated by the SEBAL algorithm and the SWAT model, the values obtained from different months of the three studied years were compared. Figure 16 gives an example of this process for the Ahvaz plain. Due to the lack of studies on the studied basin, the results of the SEBAL algorithm were compared to the NASA's satellite imagery of evapotranspiration in the ArcGIS environment. The results of this study suggested a correlation of 0.93, indicating the desirable accuracy of the SEBAL algorithm used in the study.

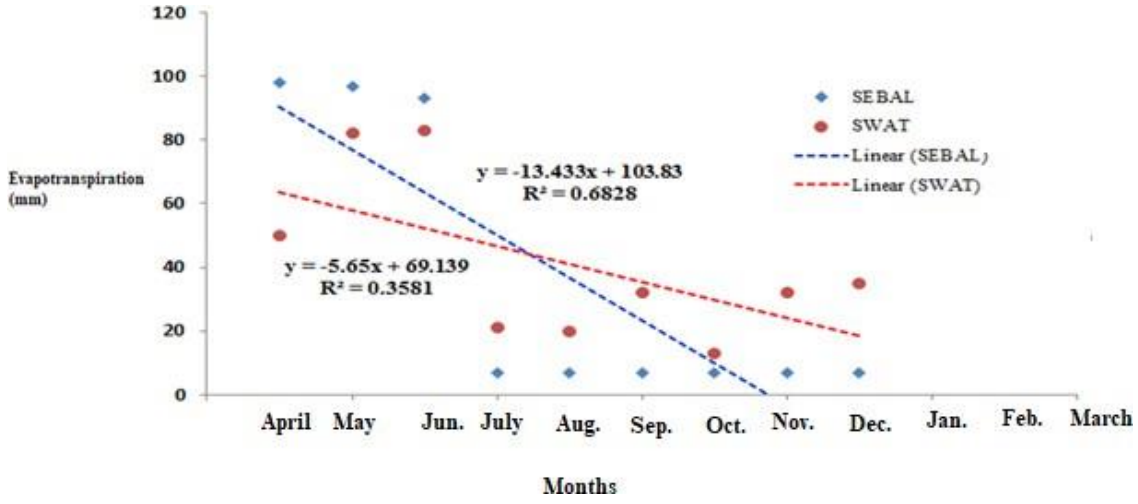

Figure 16. Comparison of evapotranspiration values taken from the SWAT model and the SEBAL algorithm in the Ahvaz plain (normal water year).

In the next stage, four plains located in the northwest (Ahvaz), east (Ahvaz Molla Sani), northeast (Hamidiyeh) and south (Sousangerd) of the basin were selected and their evapotranspiration values, obtained from SEBAL and SWAT methods, were compared based on the plains and their water year status, as shown in Figure 17.

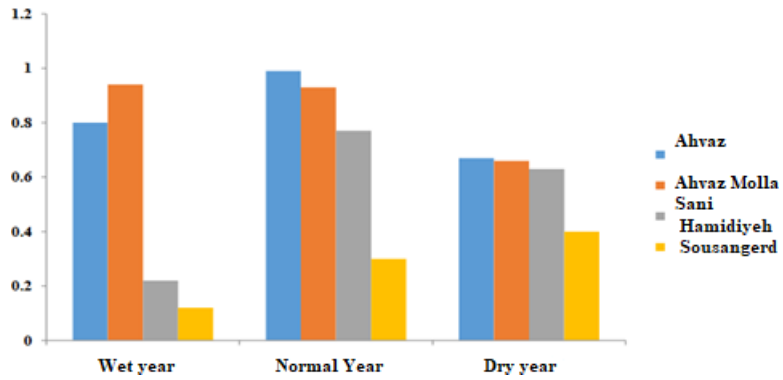

Figure 17. Comparison of the correlation of evapotranspiration values taken from the SWAT model and the SEBAL algorithm in the drainage basin's plains.

As shown by Figure 17, the correlation values between the results of the SWAT model and those of the SEBAL algorithm, as based on the water year status, were 0.72, 0.58 and 0.49, respectively for the three normal, wet and dry years. It is thus concluded that the results of the SWAT model and the SEBAL algorithm in the normal water year were closer to each other compared to the results in the wet and dry years; for this, these results can be closer to actual values.

In the final stage of the study, following the comparison of the results obtained in the previous section, the accuracy of the SEBAL algorithm results, the application of OLI sensing images of the Al-Baji plain taken from the LandSat8 satellite in 2020 (Figure 18) and the MODIS sensing images of the Ahvaz Molla Sani plain taken from the Terra satellite for the same year (Figure 18) were investigated. Because of their appropriate daily temporal separation resolution power, MODIS images are suitable to examine the daily evapotranspiration of farmlands; meanwhile, LandSat8 images, although having 16-day temporal resolution power, will be suitable due to their 30-m spatial resolution on spectral bands and 60-m spatial resolution on thermal bands, and they can better separate farmlands. The Al-Baji plain has a higher area under cultivation and smaller topographic changes, and the SWAT software's simulation of the crop yield in the Ahvaz Molla Sani plain has produced better results. On the other hand, the reason why the above-mentioned time intervals were selected was because of the absence of clouds in the images, the maximum crop growth and also the presence of ground data taken from the area under study in the time intervals. To perform the SEBAL equation operations, various parameters can be used. In the following, the maps of the main parameters in the SEBAL equation are shown. The equations related to the parameters are also provided in the above-mentioned manual.

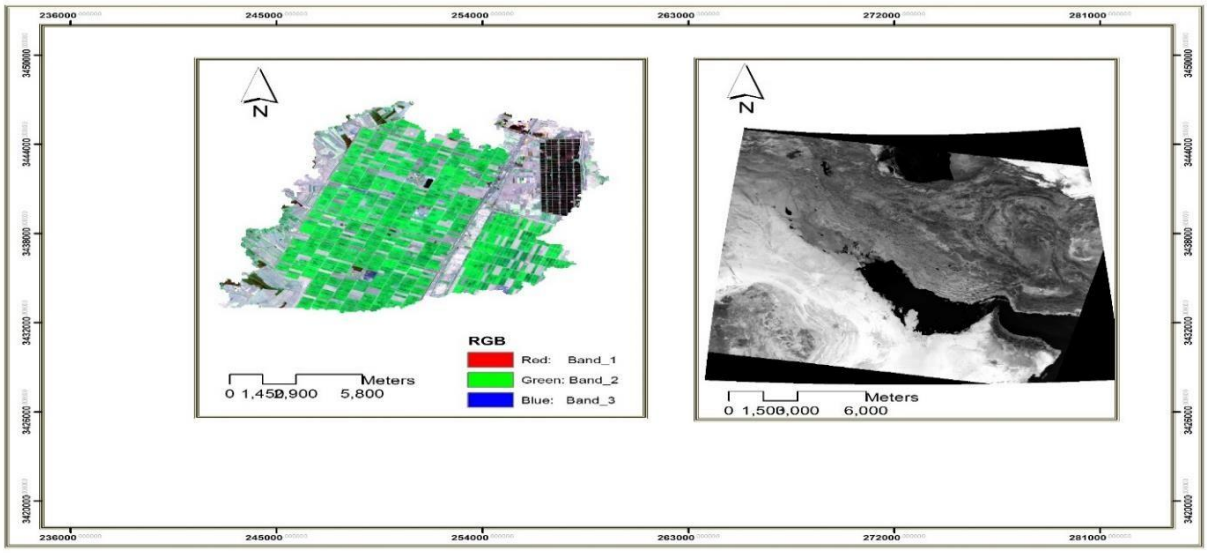

Figure 18. MODIS (right) and LandSat (left) images in 2020 (normal).

Calculating the Total Radiant Flux (Rn)

The difference between the radiation coming into and the radiation reflected from Earth's surface is called the total radiant flux, and its levels depend on many factors. The following gives a relevant map. Depending on the surface, Rn values can vary from 100 to 700 W/m2. The negative values shown in Figure 19 are due to the model's errors in some of the image pixels, as no such errors can be seen in farmlands. This completes the first stage in the SEABL method. In the second stage of the SEBAL method, it is required to obtain G and H equations to calculate the residual energy amount of evapotranspiration. The net radiant flux (Rn), as shown in Equation (13), is a net amount of radiation energy on the surface accessible for heating soil, heating the air or evaporating soil moisture. As a surface energy budget equation, it is written as follows:

$$R_n = G + H + \lambda ET \quad (13)$$

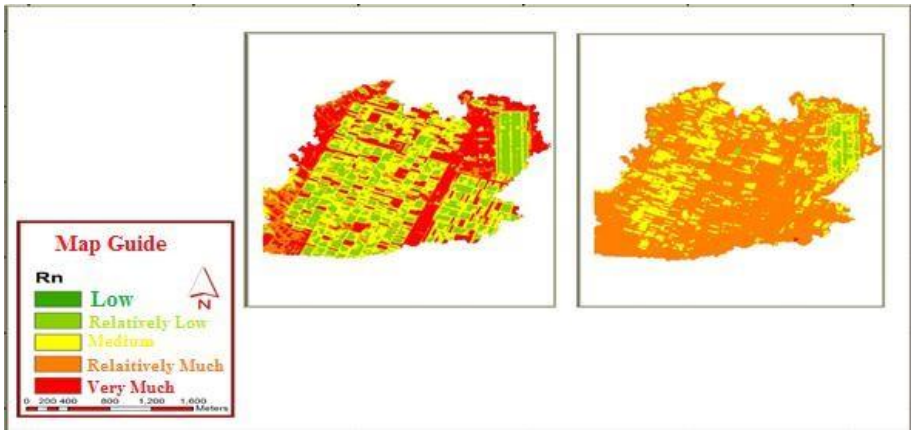

Figure 19. Surface net radiant flux of MODIS (right) and LandSat (left) images.

The range of surface net radiation changes varies from 200 to 1000 MW. This amount is lower for farmlands compared to other lands (Calculation flowchart of net solar radiation, Bastiaanssen et al. 1998).

Actual Evapotranspiration

Actual evapotranspiration is obtained from the moment the satellite passes over the area and following the calculation of unknown values in the energy balance equation. Unknown values, as suggested above, include $R_n = G + H + \lambda ET$. The following shows the calculation of hourly and daily evapotranspiration using the SEBAL model.

Figure 20 shows that the hourly evapotranspiration obtained from the Ahvaz Molla Sani and Al-Baji plains are almost close to each other. The maximum and minimum values of the actual hourly evapotranspiration based on the MODIS images in the Ahvaz Molla Sani plain are -0.75 and 1.631, while the maximum and minimum values of the actual hourly evapotranspiration based on the LandSat images in the Al-Baji Sani plain are -0.46 and 1.423, respectively, which are close to each other. Using the SEBAL algorithm, negative values are due to the model's errors in some image pixels, while values higher than 1 may pertain to plains' crops.

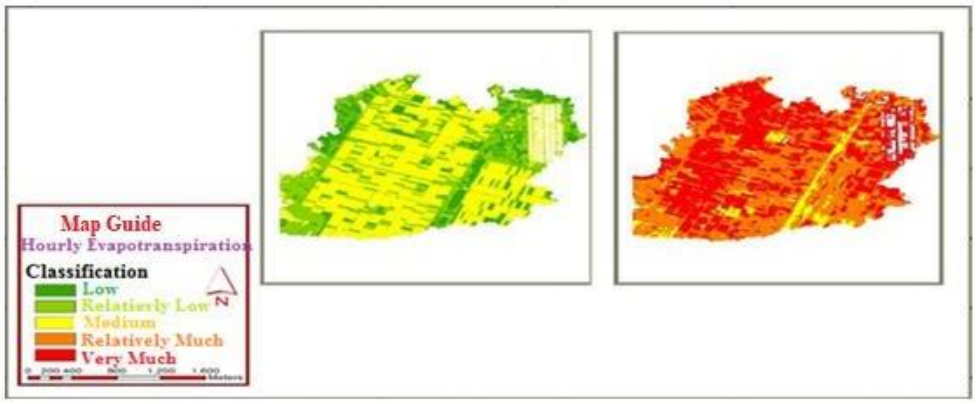

Figure 20. Map of actual hourly evapotranspiration of MODIS (right) and Landsat (left) images.

Daily Evapotranspiration

As said, the energy balance equation's unknown variables are determined before the actual evapotranspiration is computed. The sensible radiation flux (H), the instantaneous evaporation latent heat flux (IHT), the net radiation flux (Rn), and the soil heat flux (G) are among the unknown quantities in the SEBAL algorithm equations. Later, daily evapotranspiration is calculated. Daily evapotranspiration values (ET24) are usually more effective than hourly evapotranspiration (ETh). Daily evapotranspiration (ET24) is calculated from the following equation:

$$ET_{24}=ETRF\times ET_{r-24} \quad (14)$$

Figure 21 shows the output data of the 24-hour evapotranspiration for the year under study.

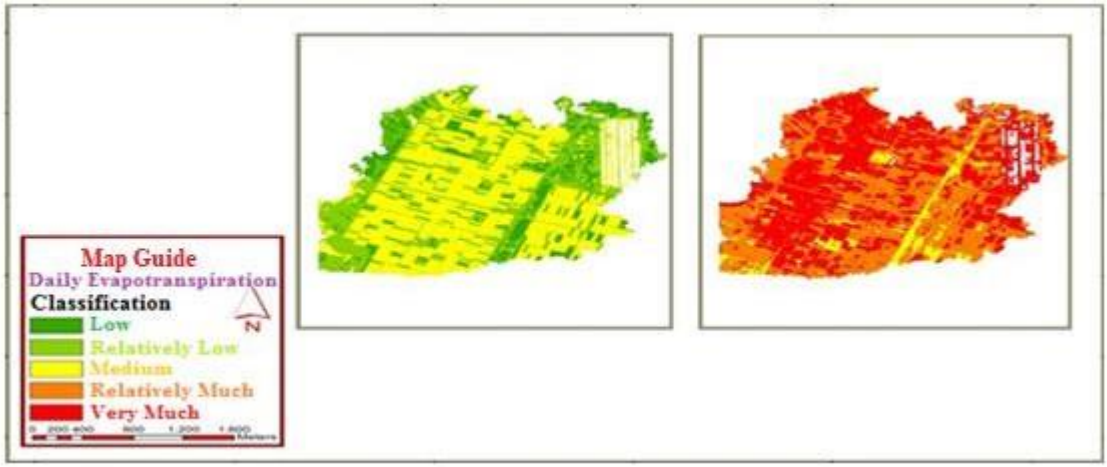

Figure 21. Daily actual evapotranspiration.

As shown by Figure 21, the maximum and minimum daily actual evapotranspiration obtained by MODIS and LandSat imagery are 3.17 and 14.26, respectively. According to the calculations, the daily evapotranspiration was found to be more applicable than the instantaneous evapotranspiration.

Hydrological Model Optimization

This study performed algorithm code-writing in the MATLAB software to investigate optimization results using the aforementioned algorithms. The results of the code-writing in the software with 10 stages of running and 100 iterations in each stage are given in Table 5. It should be stated that these values were compared to each other and to the optimal absolute response (19.41), obtained from the SUFI-2 by the SWAT-CUP software. This method takes into consideration all the uncertainties, including input uncertainty, the conceptual model, parameters and the measured data in the modeling. Hence, the average response from the honey badger algorithm is 92% of the optimal absolute response and the average billiards algorithm responses is 84% of the optimal absolute response. Moreover, the change coefficient of the honey badger algorithm is 1.43 times smaller than the billiards algorithm. These findings indicate the better performance and quality of the responses obtained from the honey badger responses in achieving optimal relative values. After calibration, the best values of the two objective functions (i.e., NS and NS-Log criteria) in the calibration period are shown by Figure 22.

Table 5. Comparison of evolutionary algorithms in optimizing the hydrological model.

	BOA Algorithms		**HBA** Algorithms	
The running step in the software	Optimal values	Run-time in seconds	Optimal values	Run-time in seconds
1	22.85	185	21.20	180
2	23.09	183	20.90	179
3	23.10	184	21.34	181
4	23.08	183	21.16	179

5	23.07	185	21.10	179
6	23.12	185	21.20	178
7	23.07	186	21.90	180
8	23.75	182	21.15	179
9	23.09	185	21.00	178
10	23.10	185	21.98	179
Average	23.132	184.3	21.09	179.2
Worst response	23.80	186	21.34	181
Best response	22.90	182	21.90	178
Coefficient of changes	0.010		0.007	
Optimal absolute response		19.41		
Percentage of closeness to the optimal absolute response	84%		92%	

As shown by Figure 22, since the minimum honey badger algorithm optimization values are much more appropriate than the optimization values of other algorithms, the honey badger algorithm's improved performance can be easily noted in gaining more minimal values (Figure 23).

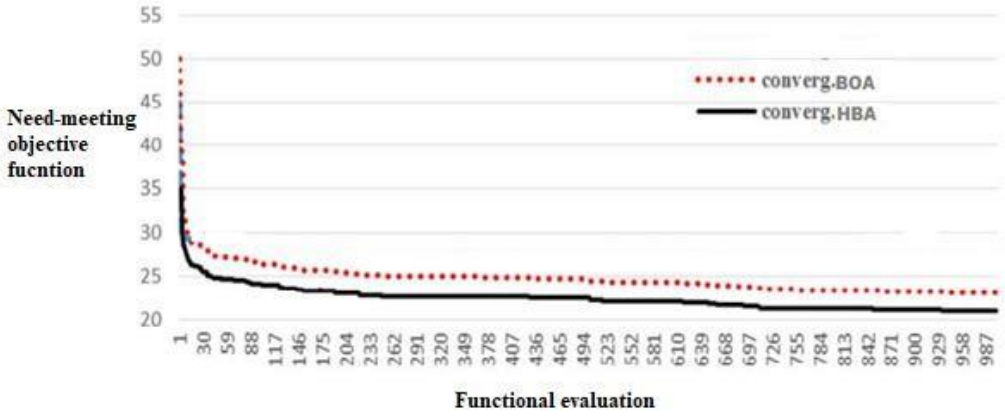

Figure 22. Convergence of responses in the applied optimization algorithms.

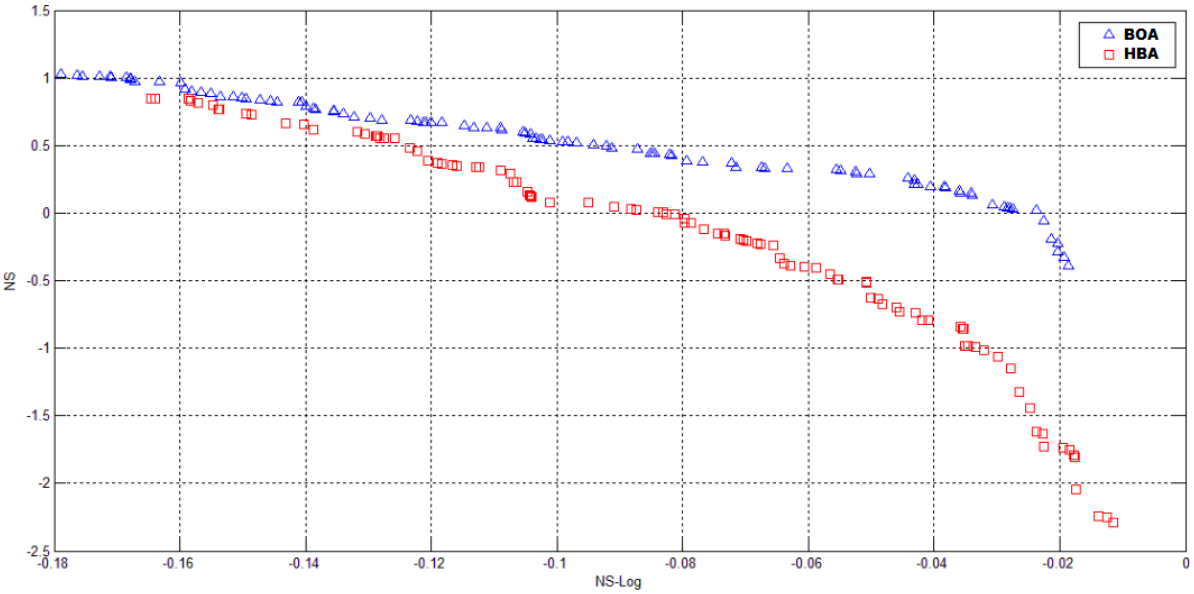

Figure 23. Pareto chart obtained by HBA and BOA algorithms in the calibration period of time.

The responses obtained by the HBA were found to be better than those of the BOA, because the HBA's NS values were higher. According to the results, NS values are generally in the range of -2.3 and 0.75 and NS-Log values in the range of -0.165 and -0.1. This indicates that the calibrated model has worked more successfully in simulating lower discharges. Output hydrographs obtained from calibrating the SWAT model in the Karun drainage basin are shown by Figure 24.

As noted, discharge values in the figures pertain to 1979 and 2017, with discharge values of 1976 to 1979 not taken into consideration. In fact, because the model was run in a continuous manner, the simulation results in these three years were considered as a warm-up period. Here, according to the figure, the range of the output hydrographs that corresponds to the optimal responses on the Pareto chart, as obtained by the HBA and BOA algorithms, are shown for the entire calibration period, as for each time, the minimum and maximum values of the simulated discharge corresponding to a set of Pareto chart points are calculated and their distance are presented in a completely tangible form, as shown by Figures 24 and 25. It is noteworthy that each point of the Pareto chart corresponds to a series of SWAT problem decision variables and a flow discharge amount at the basin's outlet. As noted, the band width of the hydrograph obtained from the HBA algorithm is partly smaller than that of the BOA's hydrograph, which is specifically due to the quality of search and parameters of these two algorithms. This suggests that the HBA algorithm behaves differently from the BOA algorithm in solving the SWAT model calibration problem in the Karun drainage basin.

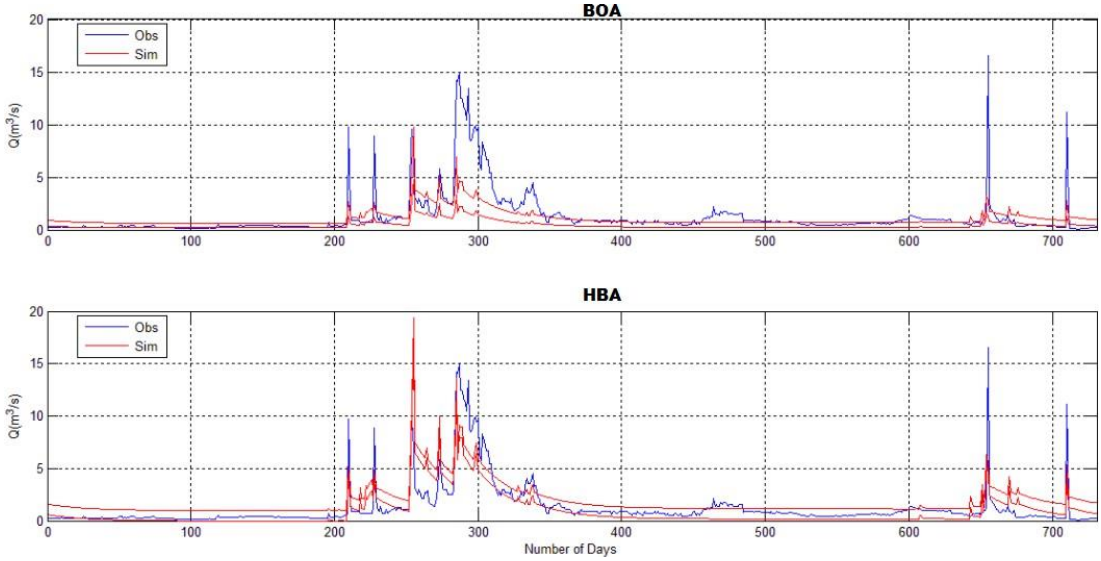

Figure 24. Output hydrographs obtained from calibrating the SWAT model in the Karun drainage basin for the calibration period.

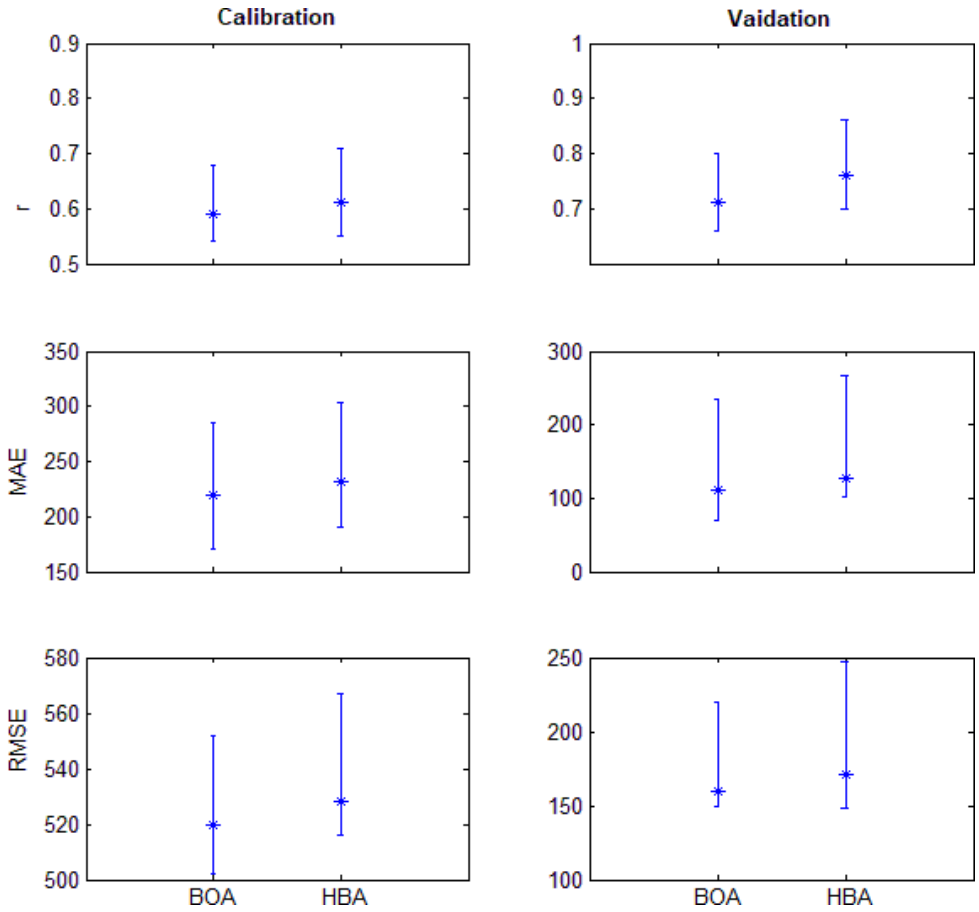

Figure 25. Minimum, maximum and average values of the criteria for measuring the quality of the simulations in the calibration of the SWAT model using various algorithms (left-to-right figures pertain to calibration and validation periods, respectively).

Figure 25 shows the correlation coefficient criteria, the average absolute value of error, and the RMSE values for the two algorithms. As noted from the figure, the HBA method, as compared to the BOA method, enjoys higher desirability concerning the statistics under investigation. This algorithm falls under appropriate methods for solving multi-objective problems, showing higher desirability in this case, too.

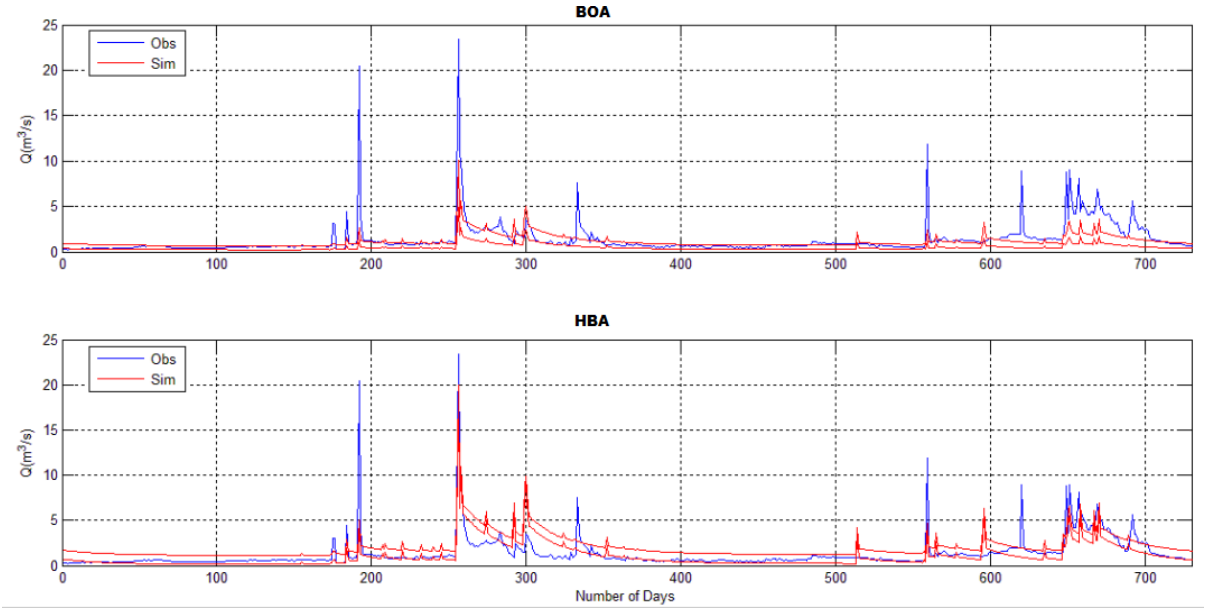

Figure 26. Output hydrographs obtained from calibrating the SWAT model in the Karun drainage basin for validation.

Figure 26 shows the simulated output hydrographs corresponding to the HBA and BOA algorithms for the years 2017-2022 in the validation period. As noted, the simulated discharge band is widened to a significant level. A comparison of the results indicates that the bandwidth of the BOA results is greater than the results of the HBA, which has caused the majority of the observational values to be within the band results. Meanwhile, the HBA results, at some times, do not compensate for the observational values of the flow discharge. Although the quality of the results obtained from the validation period was sometimes better than the calibration period, as shown by Figure 23. However, some responses were found in the responses of Figure 26 that do not enjoy good quality, including maximum discharges, being outside the band in some cases.

Results showed that the model would predict the occurrence of floods; however, the accuracy of predictions at some points cannot be so much satisfactory.

A study of the diagrams and index values showed that the optimization of the SWAT hydrological model using remote-sensing data of the SEBAL satellite and the evolutionary honey badger algorithm for determining the actual evapotranspiration of the Karun basin were far more successful and enjoyed higher desirability than ground data and other metaheuristic algorithms.

Conclusions

This study aimed to use the SEBAL algorithm and the SWAT model, calibrated by the optimization algorithms of BOA and HBA, to calculate the actual evapotranspiration values of the Karun drainage basin. The SEBAL algorithm is widely used to estimate the surface evapotranspiration and it uses remote-sensing data for this. The SWAT model has also been developed as a comprehensive model for relevant studies. In general, the results from running the two methods, optimized by the meta-heuristic algorithms, indicate the great accuracy and performance of the models in simulating the evapotranspiration values of the drainage basins. For this, [models] can be used as management measures across drainage basins. Results also suggested that the optimization of the SWAT hydrological model using remote-sensing data of the SEBAL satellite and the evolutionary honey badger algorithm for determining the actual evapotranspiration of the Karun basin were far more successful than ground data and other metaheuristic algorithms and enjoyed higher desirability. In sum, in order to optimally manage water resources and optimize the hydrological model using evapotranspiration remote-sensing data, it is advised to apply optimization algorithms of honey badger to estimate the levels of evapotranspiration so that it would help to optimally use the existing water resources and avoid the wastage of water. Finally, it is recommended that hybrid and other novel algorithms be used to evaluate their efficiency in managing water resources, especially under climate change conditions.

Funding: None.

Conflict of interest: The authors declare that they have no conflict of interest.

Data Availability Statement: The data related to the results of this study are available upon request from the corresponding author.

References

[1] Abbaspour, K.C., 2011. *User Manual for SWAT-CUP4. SWAT Calibration and Uncertainty Analysis Programs.* Swiss Federal Institute of Aquatic Science and Technology. Eawag, Duebendorf, Switzerland. http://www.eawag.ch.

[2] Allen, R.G., Pereira, L.S., Raes D. and Smith, M., 1998. Crop evapotranspiration Guidelines for computing crop water requirements. FAO irrigation and drainage Paper 56.11.

[3] Arnold, J.G., Williams, J.R., Nicks, A.D. and Sammons, N.B., 1990. *SWRRB: Abasin scale simulation model for soil and water resources management.* Texas AandM Univ. Press, College Station, TX.

[4] Bastiaanssen, W.G., Menenti, M., Feddes, R.A. and Holtslag, A.A., 1998. A remote sensing surface energy balance algorithm for land (SEBAL): 1, Formulation. *Journal of Hydrology*, 1998, 198-212.

[5] Hong, S., Hendrickx, J.M.H. and Borchers, B., 2009. Up-scaling of SEBAL derived evapotranspiration maps from Landsat (30 m) to MODIS (250 m) scale. *Journal of Hydrology*, 370, 122-138.

[6] Hooghoudt, S.B., 1940. Bijdrage tot de kennis van enige natuurkundige grootheden van de grond. *Verslag van de Landbouw- en Visserijraad*, 46, 515-707.

[7] Immerzeel, W. and Droogers, P., 2008. Calibration of a distributed horological model based on satellite evapotranspiration. *Journal of Hydrology*, 2008, 411- 424.

[8] Mir Yaeghub Zadeh, M., 2014. Developing the semi-distributed SWAT model in the evapotranspiration parameter using the energy balance algorithm (SEBAL). MSc thesis. (In Persian)

[9] Moazami Goudarzi F., Sarraf, A.P. and Ahmadi, H., 2021. Calibration of SWAT and three data-driven models for monthly stream flow simulation in Maharlu Lake Basin. *Water Supply*, 21 (8), 4219-4238.

[10] Ruhoff, A., Paz, A., Collischonn, W., Aragao, L., Rocha, H. and Malhi, Y., 2012. A MODIS-based energybalance to estimate evapotranspiration for clear-sky days in Brazilian tropical savannas. *Remote Sensing*, 4, 703-725.

[11] Sarraf A.P. and Ghasemi, H., 2021. Calibration of IHACRES Hydrological Model Using Social Spider and Search and Rescue Multi-Objective Optimization Algorithm. *Hydrogeomorphology*, 8(28), 81-105.

[12] Sarraf, A.P., and Ghasemi, H., 2022. Calibration of WetSpa Model using Black Widow Spider and Social Spider Multi-Objective Optimization Algorithms. *Environmental Erosion Research Journal*, 46 (2), 205-229.

[13] Satarzadeh, E., Sarraf, A.P., Hajikandi, H. and Sadeghian, M.S., 2022. Flood hazard mapping in western Iran: assessment of deep learning vis-à-vis machine learning models. *Natural Hazards*, 111 (2), 1355-1373.

[14] Singh, R., Kumar, S., Nangare, D. and Meena, M., 2009. Drip irrigation and black polyethylene mulch influence on growth, yield and water-use efficiency of tomato. *African Journal of Agricultural Research*, 4, 1427-1430.

[15] Soleimanipour, M. and Sarraf, A.P., 2020. "Evaluating the effects of climate change on Lar Basin Water Resources Using SWAT Model and comparing its results with Bayesian Networks and Hybrid Intelligent Models. *National Geographic*, 13 (50), 61-79.

[16] Tasumi, M., Allenm, R. and Trezza, R., 2008. At-surface albedo from Landsat and MODIS satellites for use in energy balance studies of evapotranspiration. *Journal of Hydrology*, 2008, 51- 63.

[17] Trezza, R. and Allen, R., 2003. Crop water requirements from a remote sensing model for the Snake plain area in Idaho Geoenseñanza, año/vol. 8, número 001 Universidad de los Andes San Cristobal, Venezuela. *Geoensenanza*, 8, 83-90.

[18] Walters, R., Allen, R., Tasumi, M., Trezza, R. and Bastiaanssen, W., 2002. *SEBAL, Surface Energy Balance Algorithms for Land.* Advanced Training and User Manual. Version 1.

[19] Wei, X., Sritharan, S., Kandiah, R., Osterberg, J., Neale, C. and Farrow, K., 2012. Implication of SEBAL algorithm with Landsat thematic mapper 5 in lower Colorado River basin. *Remote Sensing in Hydrology*, 2012, 98- 101.